A Real-Valued 2D DOA Estimation Algorithm of Noncircular Signal via Euler Transformation and Rotational Invariance Property

Chen Xueqiang[1,2*], *Wang Chenghua*[1,2], *Zhang Xiaofei*[1,2]

1. Key Laboratory of Radar Imaging and Microwave Photonics, Nanjing University of Aeronautics and Astronautics, Nanjing 210016, P. R. China;
2. College of Electronic and Information Engineering, Nanjing University of Aeronautics and Astronautics, Nanjing 210016, P. R. China

(Received 9 October 2015; revised 19 April 2016; accepted 26 April 2016)

Abstract: The problem of two-dimensional (2D) direction of arrival (DOA) estimation for double parallel uniform linear arrays is investigated in this paper. A real-valued DOA estimation algorithm of noncircular (NC) signal is proposed, which combines the Euler transformation and rotational invariance (RI) property between subarrays. In this work, the effective array aperture is doubled by exploiting the noncircularity of signals. The complex arithmetic is converted to real arithmetic via Euler transformation. The main contribution of this work is not only extending the NC-Euler-ESPRIT algorithm from uniform linear array to double parallel uniform linear arrays, but also constructing a new 2D rotational invariance property between subarrays, which is more complex than that in NC-Euler-ESPRIT algorithm. The proposed 2D NC-Euler-RI algorithm has much lower computational complexity than 2D NC-ESPRIT algorithm. The proposed algorithm has better angle estimation performance than 2D ESPRIT algorithm and 2D NC-PM algorithm for double parallel uniform linear arrays, and is very close to that of 2D NC-ESPRIT algorithm. The elevation angles and azimuth angles can be obtained with automatically pairing. The proposed algorithm can estimate up to $2(M-1)$ sources, which is two times that of 2D ESPRIT algorithm. Cramer-Rao bound (CRB) of noncircular signal is derived for the proposed algorithm. Computational complexity comparison is also analyzed. Finally, simulation results are presented to illustrate the effectiveness and usefulness of the proposed algorithm.

Key words: array signal processing; direction of arrival (DOA) estimation; noncircular signal; Euler transformation

CLC number: TN911.7 **Document code**: A **Article ID**: 1005-1120(2018)03-0437-12

0 Introduction

The problem of estimating the direction-of-arrival (DOA) of multiple sources in the field of array signal processing has received considerable attention for decades[1-3]. Various DOA estimation algorithms have been developed and applied in many fields, including mobile communication system, radio astronomy, sonar and radar[4-6]. Although the maximum likelihood estimator[7-8] provides the optimum parameter estimation performance, its computational complexity is extremely high. Suboptimal but simpler solutions can be achieved by subspace based approaches, which rely on the decomposition of observation space into signal subspace and noise subspace. For example, both multiple signal classification (MUSIC) method[9] and estimation of signal parameters via rotational invariance technique (ESPRIT) [10] are well-known subspace based directions of arrival estimation algorithm for their good angle estimation performance.

Noncircular signals have received considera-

* Corresponding author, E-mail address: cxq2008@nuaa.edu.cn.

How to cite this article: Chen Xueqiang, Wang Chenghua, Zhang Xiaofei, et al. A real-valued 2D DOA estimation algorithm of noncircular signal via Euler transformation and rotational invariance property[J]. Trans. Nanjing Univ. Aero. Astro., 2018,35(3):437-448.
http://dx.doi.org/10.16356/j.1005-1120.2018.03.437

ble attention in the field of spatial spectrum estimation[11]. The amplitude modulation (AM) and binary phase shift keying (BPSK) modulated signals frequently used in communication systems are noncircular (NC) signals[12]. The noncircularity of signal is investigated to enhance the performance of angle estimation algorithm by combing array output and its conjugated counterpart. Some noncircular DOA estimation methods of multiple signals have been reported, such as NC-MUSIC algorithm[13], NC-ESPRIT algorithm[14], NC-propagator methods (NC-PM)[15-16], and NC-parallel factor (NC-PARAFAC) algorithm[17]. These noncircular DOA estimation algorithms have better angle estimation performance and can estimate more sources.

However, the arithmetic of the above mentioned DOA estimation algorithms is operated in complex field. Thus the corresponding computational complexity is very high. Huarng and Yeh have proposed real-valued MUSIC algorithm[18] and real-valued ESPRIT algorithm[19] by unitary transformation, respectively. A real-valued noncircular ESPRIT algorithm for uniform linear array has been proposed in Ref. [20], which has lower computational complexity than NC-ESPRIT[14] algorithm. Then this method is extended to PM algorithm for two-dimensional (2D) angle estimation by Zhang[21].

In this paper, a computationally efficient 2D angle estimation algorithm of noncircular signal for double parallel uniform linear arrays via Euler transformation and rotational invariance property between subarrays (2D NC-Euler-RI) is proposed. The complex arithmetic in this work is converted to real arithmetic by Euler transformation. The main contribution of this work is not only extending the NC-Euler-ESPRIT algorithm[20] from uniform linear array to double parallel uniform linear arrays, but also constructing a new 2D rotational invariance property between subarrays, which is more complex than that in NC-Euler-ESPRIT algorithm. Moreover, the proposed 2D NC-Euler-RI algorithm needs to consider matching problem between elevation angles and azimuth angles. We also analyze the computational complexity of the proposed algorithm and derive the CRB of noncircular signal for double parallel uniform linear arrays.

The proposed algorithm has the following advantages: (1) It has lower computational complexity than 2D ESPRIT[10] algorithm and 2D NC-ESPRIT algorithm[14] for double parallel uniform linear arrays. (2) It can estimate up to $2(M-1)$ sources, which is two times that of NC-Euler-ESPRIT algorithm. (3) It can achieve automatically paired elevation angles and azimuth angles. (4) It has better angle estimation performance than that of 2D ESPRIT algorithm[10], 2D NC-PM algorithm[22] for double parallel uniform linear array, and close to that of 2D NC-ESPRIT algorithm[14].

Notations: $(\cdot)^{-1}$, $(\cdot)^*$, $(\cdot)^{\mathrm{T}}$, $(\cdot)^{\mathrm{H}}$, $(\cdot)^+$ denote inverse, conjugate, transpose, conjugate-transpose and pseudo-inverse operations, respectively. diag$\{\boldsymbol{v}\}$ stands for a diagonal matrix, whose diagonal elements are the elements in vector $\boldsymbol{v}$. $\boldsymbol{I}_K$ is a $K\times K$ identity matrix. $E(\cdot)$ is the expectation operator. angle$(\cdot)$ means to get the phase. Re$[\cdot]$ and Im$[\cdot]$ mean to get the real part and imaginary part of complex number, respectively.

1 Data Model

Assume that there are K uncorrelated narrowband sources impinging on double parallel uniform linear arrays, and each uniform linear subarray equipped with M sensors is shown in Fig. 1. The distance d between adjacent sensors is equivalent to half of the wavelength λ. The sources are far away from the subarrays, thus the incoming waves over the sensors are essentially planes. The noise is additive independent identically distributed Gaussian with zero mean and variance σ^2, which is uncorrelated with the signal. We denote the 2D DOAs of kth source as $\boldsymbol{\varphi}_k=[\theta_k,\varphi_k]$, where θ_k and φ_k denote elevation angle and azimuth angle, respectively, and $k=1,\cdots,K$.

The output signals of subarrays along X axis at time t can be modeled as[23]

$$\begin{cases}\boldsymbol{x}_1(t)=\boldsymbol{A}\boldsymbol{s}(t)+\boldsymbol{n}_1(t)\\ \boldsymbol{x}_2(t)=\boldsymbol{A}\boldsymbol{\Phi}_Y\boldsymbol{s}(t)+\boldsymbol{n}_2(t)\end{cases} \tag{1}$$

where $\boldsymbol{x}_1(t),\boldsymbol{x}_2(t)\in\mathbf{C}^{M\times 1}$ are the received signals of each subarray; $\boldsymbol{A}=[\boldsymbol{a}_1,\cdots,\boldsymbol{a}_k,\cdots,\boldsymbol{a}_K]\in\mathbf{C}^{M\times K}$ is the steering matrix, $\boldsymbol{a}_k=[1,\cdots,\mathrm{e}^{\mathrm{j}(m-1)\tau_{x,k}},\cdots,\mathrm{e}^{\mathrm{j}(M-1)\tau_{x,k}}]^{\mathrm{T}}$, $\tau_{x,k}=2\pi d\cdot\cos(\varphi_k)\sin(\theta_k)/\lambda$, $m=1,\cdots,M$; $\boldsymbol{s}(t)\in\mathbf{C}^{K\times 1}$; and $\boldsymbol{\Phi}_Y$ is a diagonal matrix

$$\boldsymbol{\Phi}_Y=\begin{bmatrix}\mathrm{e}^{\mathrm{j}\tau_{y,1}} & \cdots & 0\\ \vdots & \ddots & \vdots\\ 0 & \cdots & \mathrm{e}^{\mathrm{j}\tau_{y,K}}\end{bmatrix} \tag{2}$$

where $\tau_{y,k}=2\pi d\sin(\varphi_k)\sin(\theta_k)/\lambda$.

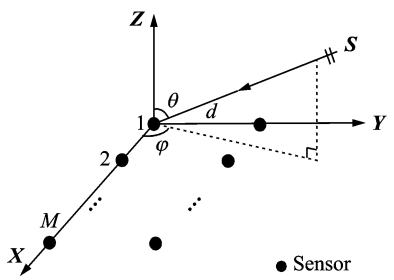

Fig. 1 Array geometry[23]

A brief definition of noncircular signal is given in the following[24]. Let $\boldsymbol{s}(t)$ be a complex random process with zero mean. The second order statistics of $\boldsymbol{s}(t)$ are defined as the covariance $E\{\boldsymbol{s}(t)\boldsymbol{s}^*(t)\}$ and conjugate covariance $E\{\boldsymbol{s}^2(t)\}$, respectively. The relationship between these two covariance measures is

$$E\{\boldsymbol{s}^2(t)\}=\rho\mathrm{e}^{\mathrm{j}\psi}E\{\boldsymbol{s}(t)\boldsymbol{s}^*(t)\} \tag{3}$$

where ψ is the noncircular phase and $\rho(\rho\in[0,1])$ denotes the noncircular rate. It is defined that $\boldsymbol{s}(t)$ is circular when $\rho=0$ and is noncircular when $0<\rho\leqslant 1$.

Only the signals of maximum noncircular rate $\rho=1$ are considered in this work. The noncircular signals $\boldsymbol{s}$(t) with maximum noncircular rate can be expressed as

$$\boldsymbol{s}(t)=\boldsymbol{\Psi}\boldsymbol{s}_0(t) \tag{4}$$

where $\boldsymbol{s}_0(t)\in\mathbf{R}^{K\times 1}$, and

$$\boldsymbol{\Psi}=\begin{bmatrix}\mathrm{e}^{\mathrm{j}\psi_1} & \cdots & 0\\ \vdots & \ddots & \vdots\\ 0 & \cdots & \mathrm{e}^{\mathrm{j}\psi_K}\end{bmatrix} \tag{5}$$

where ψ_k is the noncircular phase of kth signal and is assumed to be in the range of $[0,\pi]$.

2 Angle Estimation Algorithm

2.1 Euler transformation of array output

According to Eq. (1), define the real-valued subarray output via Euler transformation[20] as follows

$$\begin{cases}\boldsymbol{x}_{1c}(t)=[\boldsymbol{x}_1(t)+\boldsymbol{x}_1^*(t)]/2=\boldsymbol{A}_{1c}\boldsymbol{s}_0(t)+\boldsymbol{n}_{1c}(t)\\ \boldsymbol{x}_{1s}(t)=[\boldsymbol{x}_1(t)-\boldsymbol{x}_1^*(t)]/(2j)=\boldsymbol{A}_{1s}\boldsymbol{s}_0(t)+\boldsymbol{n}_{1s}(t)\\ \boldsymbol{x}_{2c}(t)=[\boldsymbol{x}_2(t)+\boldsymbol{x}_2^*(t)]/2=\boldsymbol{A}_{2c}\boldsymbol{s}_0(t)+\boldsymbol{n}_{2c}(t)\\ \boldsymbol{x}_{2s}(t)=[\boldsymbol{x}_2(t)-\boldsymbol{x}_2^*(t)]/(2j)=\boldsymbol{A}_{2s}\boldsymbol{s}_0(t)+\boldsymbol{n}_{2s}(t)\end{cases} \tag{6}$$

where $\boldsymbol{A}_{1c}$, $\boldsymbol{A}_{1s}$, $\boldsymbol{A}_{2c}$, $\boldsymbol{A}_{2c}\in\mathbf{R}^{M\times K}$, $\boldsymbol{n}_{1c}(t)=\mathrm{Re}[\boldsymbol{n}_1(t)]$, $\boldsymbol{n}_{1s}(t)=\mathrm{Im}[\boldsymbol{n}_1(t)]$, $\boldsymbol{n}_{2c}(t)=\mathrm{Re}[\boldsymbol{n}_2(t)]$, $\boldsymbol{n}_{2s}(t)=\mathrm{Im}[\boldsymbol{n}_2(t)]$.

Construct the extended real-valued array output as

$$\boldsymbol{x}_r(t)=\boldsymbol{A}_r\boldsymbol{s}_0(t)+\boldsymbol{n}_r(t) \tag{7}$$

with L snapshots can be written as

$$\boldsymbol{X}_r=\boldsymbol{A}_r\boldsymbol{S}_0+\boldsymbol{N}_r \tag{8}$$

where $\boldsymbol{X}_r\in\mathbf{R}^{4M\times L}$, $\boldsymbol{S}_0\in\mathbf{R}^{K\times L}$, $\boldsymbol{N}_r\in\mathbf{R}^{4M\times L}$.

2.2 2D NC-Euler-RI algorithm

Define

$$\boldsymbol{T}_1=\begin{bmatrix}1 & 1 & 0 & 0 & \cdots & 0\\ 0 & 1 & 1 & 0 & \cdots & 0\\ \vdots & \vdots & \vdots & \vdots & \ddots & \vdots\\ 0 & \cdots & 0 & 0 & 1 & 1\end{bmatrix} \tag{9}$$

$$\boldsymbol{T}_2=\begin{bmatrix}1 & -1 & 0 & 0 & \cdots & 0\\ 0 & 1 & -1 & 0 & \cdots & 0\\ \vdots & \vdots & \vdots & \vdots & \ddots & \vdots\\ 0 & \cdots & 0 & 0 & 1 & -1\end{bmatrix} \tag{10}$$

where $\boldsymbol{T}_1$ and $\boldsymbol{T}_2\in\mathbf{R}^{(M-1)\times M}$.

Let

$$\boldsymbol{J}_1=\begin{bmatrix}\boldsymbol{T}_1 & \boldsymbol{0} & \boldsymbol{0} & \boldsymbol{0}\\ \boldsymbol{0} & \boldsymbol{T}_1 & \boldsymbol{0} & \boldsymbol{0}\\ \boldsymbol{0} & \boldsymbol{0} & \boldsymbol{T}_1 & \boldsymbol{0}\\ \boldsymbol{0} & \boldsymbol{0} & \boldsymbol{0} & \boldsymbol{T}_1\end{bmatrix} \tag{11}$$

$$\boldsymbol{J}_2=\begin{bmatrix}\boldsymbol{0} & -\boldsymbol{T}_2 & \boldsymbol{0} & \boldsymbol{0}\\ \boldsymbol{T}_2 & \boldsymbol{0} & \boldsymbol{0} & \boldsymbol{0}\\ \boldsymbol{0} & \boldsymbol{0} & \boldsymbol{0} & -\boldsymbol{T}_2\\ \boldsymbol{0} & \boldsymbol{0} & \boldsymbol{T}_2 & \boldsymbol{0}\end{bmatrix} \tag{12}$$

where $\boldsymbol{J}_1,\boldsymbol{J}_2\in\mathbf{R}^{4(M-1)\times 4M}$.

Combining Eq. (7) and Eqs. (11), (12), we have

$$\boldsymbol{J}_1\boldsymbol{A}_r\boldsymbol{D}_1=\boldsymbol{J}_2\boldsymbol{A}_r \tag{13}$$

where

$$\boldsymbol{D}_1=\begin{bmatrix}\tan\left(\frac{\tau_{x,1}}{2}\right) & \cdots & 0\\ \vdots & \ddots & \vdots\\ 0 & \cdots & \tan\left(\frac{\tau_{x,K}}{2}\right)\end{bmatrix} \tag{14}$$

where $\boldsymbol{D}_1\in\mathbf{R}^{K\times K}$.

Define the covariance matrix of $\boldsymbol{x}_r(t)$ as[25]

$$\boldsymbol{R}_x=E[\boldsymbol{x}_r(t)\boldsymbol{x}_r^{\mathrm{T}}(t)]=\boldsymbol{A}_r\boldsymbol{R}_0\boldsymbol{A}_r^{\mathrm{T}}+\sigma^2\boldsymbol{I}_{4M} \tag{15}$$

where $\mathbf{R}_x\in\mathbf{R}^{4M\times 4M}$, $\boldsymbol{R}_0=E[\boldsymbol{s}_0(t)\boldsymbol{s}_0^{\mathrm{T}}(t)]\in\mathbf{R}^{K\times K}$.

$\boldsymbol{R}_x$ can be rewritten via Eigen value decomposition (EVD) as

$$\boldsymbol{R}_x=\boldsymbol{U}_s\boldsymbol{\Sigma}_s\boldsymbol{U}_s^{\mathrm{T}}+\boldsymbol{U}_n\boldsymbol{\Sigma}_n\boldsymbol{U}_n^{\mathrm{T}} \tag{16}$$

where $\boldsymbol{U}_s\in\mathbf{R}^{4M\times K}$, $\boldsymbol{U}_n\in\mathbf{R}^{4M\times(4M-K)}$, $\boldsymbol{\Sigma}_s\in\mathbf{R}^{K\times K}$, $\boldsymbol{\Sigma}_n\in\mathbf{R}^{(4M-K)\times(4M-K)}$.

For $\boldsymbol{U}_s$ and $\boldsymbol{A}_r$ can span the same signal subspace, it can be obtained that

$$\boldsymbol{U}_s\boldsymbol{\Pi}_1=\boldsymbol{A}_r \tag{17}$$

where $\boldsymbol{\Pi}_1$ is a nonsingular matrix, and $\boldsymbol{\Pi}_1\in\mathbf{R}^{K\times K}$.

Combine Eq. (13) and Eq. (17), and we have

$$\boldsymbol{J}_1\boldsymbol{U}_s(\boldsymbol{\Pi}_1\boldsymbol{D}_1\boldsymbol{\Pi}_1^{-1})=\boldsymbol{J}_2\boldsymbol{U}_s \tag{18}$$

Define

$$\boldsymbol{P}_1=(\boldsymbol{J}_1\boldsymbol{U}_s)^{+}\boldsymbol{J}_2\boldsymbol{U}_s \tag{19}$$

where $\boldsymbol{P}_1\in\mathbf{R}^{K\times K}$.

According to Eqs. (18), (19), we have

$$\boldsymbol{P}_1=\boldsymbol{\Pi}_1\boldsymbol{D}_1\boldsymbol{\Pi}_1^{-1} \tag{20}$$

Perform the EVD of $\boldsymbol{P}_1$, which can be expressed as

$$\boldsymbol{P}_1=\boldsymbol{V}\boldsymbol{\Lambda}\boldsymbol{V}^{\mathrm{T}} \tag{21}$$

where $\boldsymbol{V}\in\mathbf{R}^{K\times K}$, $\boldsymbol{\Lambda}=\begin{bmatrix}\gamma_1 & \cdots & 0\\ \vdots & \ddots & \vdots\\ 0 & \cdots & \gamma_K\end{bmatrix}$, γ_k is the kth diagonal element of $\boldsymbol{\Lambda}$.

Combine Eq. (14) and Eqs. (20), (21), and we have

$$\gamma_k=\tan\left(\frac{\tau_{x,k}}{2}\right) \tag{22}$$

Then reconstruct the extended real-valued array output data along Y axis as

$$\boldsymbol{y}_r(t)=\boldsymbol{B}_r\boldsymbol{s}_0(t)+\boldsymbol{n}_y(t) \tag{23}$$

where $\boldsymbol{y}_r(t),\boldsymbol{n}_y(t)\in\mathbf{R}^{4M\times 1}$, $\boldsymbol{B}_r\in\mathbf{R}^{4M\times K}$, and

$$\boldsymbol{B}_r=[\boldsymbol{B}_{1c}^{\mathrm{T}},\boldsymbol{B}_{1s}^{\mathrm{T}},\cdots,\boldsymbol{B}_{mc}^{\mathrm{T}},\boldsymbol{B}_{ms}^{\mathrm{T}},\cdots,\boldsymbol{B}_{Mc}^{\mathrm{T}},\boldsymbol{B}_{Ms}^{\mathrm{T}}]^{\mathrm{T}} \tag{24}$$

$$\boldsymbol{B}_{mc}=\begin{bmatrix}\cos(d_{m,1}+\psi_1) & \cdots & \cos(d_{m,K}+\psi_K)\\ \cos(D_{m,1}+\psi_1) & \cdots & \cos(D_{m,K}+\psi_K)\end{bmatrix} \tag{25}$$

$$\boldsymbol{B}_{ms}=\begin{bmatrix}\sin(d_{m,1}+\psi_1) & \cdots & \sin(d_{m,K}+\psi_K)\\ \sin(D_{m,1}+\psi_1) & \cdots & \sin(D_{m,K}+\psi_K)\end{bmatrix} \tag{26}$$

where $d_{m,k}=(m-1)\tau_{x,k}$, $D_{m,k}=d_{m,k}+\tau_{y,k}$.

Define

$$\boldsymbol{T}_3=[1\quad 1] \tag{27}$$

$$\boldsymbol{T}_4=[1\quad -1] \tag{28}$$

Let

$$\boldsymbol{Q}_3=\begin{bmatrix}\boldsymbol{T}_3 & \boldsymbol{0}\\ \boldsymbol{0} & \boldsymbol{T}_3\end{bmatrix} \tag{29}$$

$$\boldsymbol{Q}_4=\begin{bmatrix}\boldsymbol{0} & -\boldsymbol{T}_4\\ \boldsymbol{T}_4 & \boldsymbol{0}\end{bmatrix} \tag{30}$$

Combine Eqs. (29), (30) and construct $\boldsymbol{J}_3$, $\boldsymbol{J}_4$ as follows

$$\boldsymbol{J}_3=\begin{bmatrix}\boldsymbol{Q}_3 & \cdots & \boldsymbol{0}\\ \vdots & \ddots & \vdots\\ \boldsymbol{0} & \cdots & \boldsymbol{Q}_3\end{bmatrix} \tag{31}$$

$$\boldsymbol{J}_4=\begin{bmatrix}\boldsymbol{Q}_4 & \cdots & \boldsymbol{0}\\ \vdots & \ddots & \vdots\\ \boldsymbol{0} & \cdots & \boldsymbol{Q}_4\end{bmatrix} \tag{32}$$

where $\boldsymbol{J}_3,\boldsymbol{J}_4\in\mathbf{R}^{2M\times 4M}$.

Combine Eq. (23) and Eqs. (31), (32), and we have

$$\boldsymbol{J}_3\boldsymbol{B}_r\boldsymbol{D}_2=\boldsymbol{J}_4\boldsymbol{B}_r \tag{33}$$

where $\boldsymbol{D}_2\in\mathbf{R}^{K\times K}$, and

$$\boldsymbol{D}_2=\begin{bmatrix}\tan\left(\frac{\tau_{y,1}}{2}\right) & \cdots & 0\\ \vdots & \ddots & \vdots\\ 0 & \cdots & \tan\left(\frac{\tau_{y,K}}{2}\right)\end{bmatrix} \tag{34}$$

Define the covariance matrix of $\boldsymbol{y}_r(t)$ as[25]

$$\boldsymbol{R}_y=E[\boldsymbol{y}_r(t)\boldsymbol{y}_r^{\mathrm{T}}(t)]=\boldsymbol{B}_r\boldsymbol{R}_0\boldsymbol{B}_r^{\mathrm{T}}+\sigma^2\boldsymbol{I}_{4M} \tag{35}$$

where $\boldsymbol{R}_y\in\mathbf{R}^{4M\times 4M}$.

$\boldsymbol{R}_y$ can be rewritten via EVD as

$$\boldsymbol{R}_y=\boldsymbol{B}_s\boldsymbol{\Delta}_s\boldsymbol{B}_s^{\mathrm{T}}+\boldsymbol{B}_n\boldsymbol{\Delta}_n\boldsymbol{B}_n^{\mathrm{T}} \tag{36}$$

where $\boldsymbol{B}_s\in\mathbf{R}^{4M\times K}$, $\boldsymbol{B}_n\in\mathbf{R}^{4M\times(4M-K)}$, $\boldsymbol{\Delta}_s\in\mathbf{R}^{K\times K}$, $\boldsymbol{\Delta}_n\in\mathbf{R}^{(4M-K)\times(4M-K)}$.

For $\boldsymbol{B}_s$ and $\boldsymbol{B}_r$ can span the same signal subspace, it can be obtained that

$$\boldsymbol{B}_s\boldsymbol{\Pi}_2=\boldsymbol{B}_r \tag{37}$$

where $\boldsymbol{\Pi}_2\in\mathbf{R}^{K\times K}$ is a noncircular matrix.

Combine Eq. (33) and Eq. (37), and we have

$$\boldsymbol{J}_3\boldsymbol{B}_s(\boldsymbol{\Pi}_2\boldsymbol{D}_2\boldsymbol{\Pi}_2^{-1})=\boldsymbol{J}_4\boldsymbol{B}_s \tag{38}$$

Define

$$\boldsymbol{P}_2 = (\boldsymbol{J}_3\boldsymbol{B}_s)^+ \boldsymbol{J}_4\boldsymbol{B}_s \tag{39}$$

where $\boldsymbol{P}_2 \in \mathbf{R}^{K\times K}$.

According to Eqs. (38), (39), we have

$$\boldsymbol{P}_2 = \boldsymbol{\Pi}_2\boldsymbol{D}_2\boldsymbol{\Pi}_2^{-1} \tag{40}$$

Perform the EVD of $\boldsymbol{P}_2$, which can be rewritten as

$$\boldsymbol{P}_2 = \boldsymbol{H}\boldsymbol{\Omega}\boldsymbol{H}^{\mathrm{T}} \tag{41}$$

where $\boldsymbol{H} \in \mathbf{R}^{K\times K}$, $\boldsymbol{\Omega} = \begin{bmatrix} \omega_1 & \cdots & 0 \\ \vdots & \ddots & \vdots \\ 0 & \cdots & \omega_K \end{bmatrix}$, ω_k is the kth diagonal element of $\boldsymbol{\Omega}$.

Combining Eqs. (40), (41), it can be obtained that

$$\omega_k = \tan\left(\frac{\tau_{y,k}}{2}\right) \tag{42}$$

Note that the EVDs of $\boldsymbol{P}_1$ and $\boldsymbol{P}_2$ are performed, respectively. We should consider the column ambiguity and scale fuzzy between $\boldsymbol{\Lambda}$ and $\boldsymbol{\Omega}$ before estimating the DOAs. According to Eqs. (7), (23), $\boldsymbol{y}_r(t)$ can be obtained by row elementary transformation of $\boldsymbol{x}_r(t)$, so $\boldsymbol{B}_s$ can be achieved as follow

$$\boldsymbol{B}_s = \boldsymbol{J}_0\boldsymbol{U}_s \tag{43}$$

where $\boldsymbol{J}_0$ is the row elementary transformation matrix.

Then replace $\boldsymbol{\Pi}_2$ in Eq. (40) with

$$\boldsymbol{\Pi}'_2 = \boldsymbol{\Pi}_2\boldsymbol{\Pi}_1 \tag{44}$$

The column ambiguity and scale fuzzy between $\boldsymbol{\Lambda}$ and $\boldsymbol{\Omega}$ can be solved.

Define that

$$\mu_k = \cos(\varphi_k)\sin(\theta_k) \tag{45}$$

$$\eta_k = \sin(\varphi_k)\sin(\theta_k) \tag{46}$$

Thus the estimates of μ_k and η_k are

$$\hat{\mu}_k = \lambda \cdot \arctan\frac{\gamma_k}{\pi d} \tag{47}$$

$$\hat{\eta}_k = \lambda \cdot \arctan\frac{\omega_k}{\pi d} \tag{48}$$

Therefore, the azimuth angles and elevation angles can be estimated as follows

$$\hat{\varphi}_k = \arctan\left(\frac{\hat{\eta}_k}{\hat{\mu}_k}\right) \tag{49}$$

$$\hat{\theta}_k = \arcsin\sqrt{\hat{\eta}_k^2 + \hat{\mu}_k^2} \tag{50}$$

2.3 Algorithm description

The implementation of the proposed algorithm with finite array output data is summarized in this section. The sampled covariance matrices $\hat{\boldsymbol{R}}_x$ with L snapshots are defined as[26]

$$\hat{\boldsymbol{R}}_x = \frac{1}{L}\sum_{l=1}^{L}\boldsymbol{x}_r(t_l)\boldsymbol{x}_r^{\mathrm{T}}(t_l) \tag{51}$$

The procedure of the proposed 2D NC-Euler-RI algorithm for double parallel uniform linear arrays is presented in the following.

(1) Initialize the sampled array output data of subarrays $\boldsymbol{X}_1$, $\boldsymbol{X}_2$, and define the matrices $\boldsymbol{J}_0$, $\boldsymbol{J}_1$, $\boldsymbol{J}_2$, $\boldsymbol{J}_3$, $\boldsymbol{J}_4$.

(2) Construct the extended real-valued array output $\boldsymbol{X}_r$ via Euler transformation.

(3) Compute the corresponding sampled covariance matrix $\hat{\boldsymbol{R}}_x$, and perform the EVD of $\hat{\boldsymbol{R}}_x$.

(4) Extract the signal subspace $\boldsymbol{U}_s$, and reconstruct $\boldsymbol{U}_s$ to get $\boldsymbol{B}_s$ via Eq. (43).

(5) Compute the matrices $\boldsymbol{P}_1$ and $\boldsymbol{P}_2$, and perform the EVD of $\boldsymbol{P}_1$ and $\boldsymbol{P}_2$, respectively.

(6) Estimate the elevation angles and azimuth angles via Eqs. (49), (50).

Remark 1 It is assumed that the number of sources is pre-known, or it can be estimated by some methods shown in Refs. [27-29].

Remark 2 The column ambiguity and scale fuzzy between $\boldsymbol{\Lambda}$ and $\boldsymbol{\Omega}$ are solved via Eqs. (47), (48). Thus the elevation angles and azimuth angles can be obtained with automatic pairing.

2.4 Analysis of complexity

Regarding the computational complexity, only matrix multiplication operations are considered. The complexities of 2D ESPRIT algorithm[10], 2D NC-ESPRIT algorithm[14] and the proposed 2D NC-Euler-RI algorithm for double parallel uniform linear arrays are analyzed in Table 1. Fig. 2 is the simulation results of computational complexity comparison among 2D ESPRIT algorithm, 2D NC-ESPRIT algorithm and 2D NC-Euler-RI algorithm with different numbers of snapshots L and sensors M. It can be seen that the proposed 2D NC-Euler-RI algorithm has

Table 1 Computational complexity of three methods for double parallel uniform linear arrays

Algorithm	Computational complexity
2D-ESPRIT	$4M^2L+8M^3+3K^2(3M-2)+2K^3$
2D-NC-ESPRIT	$16(5M^2-8M+4)L+6K^2(5M-4)+2K^3$
2D-NC-Euler-RI	$4M^2L+16M^3+3K^2(5M-4)+\frac{K^3}{2}+4ML$

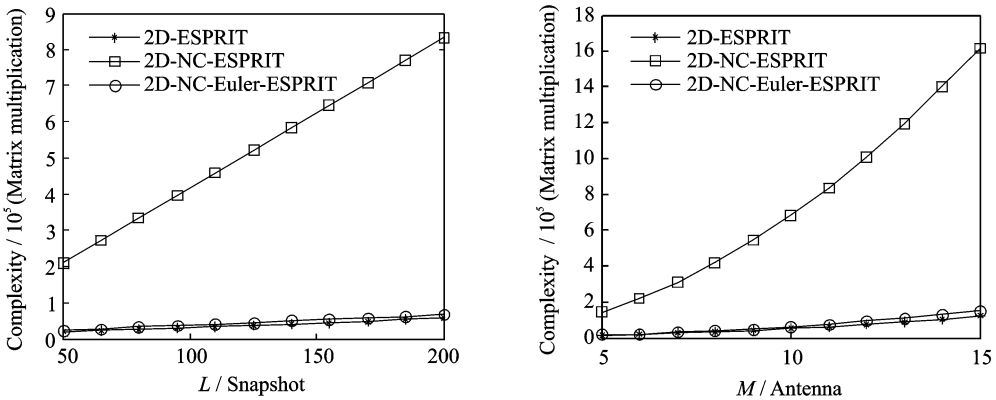

Fig. 2 Simulation results of complexity comparison with different values of L and M

much lower computational complexity of than that of 2D NC-ESPRIT algorithm, and close to that of 2D ESPRIT algorithm.

Note that the dimension of array output data is doubled by exploiting the noncircularity of signal. The effective array aperture of the proposed algorithm is $2M$, which is two times that of ESPRIT algorithm. Thus the proposed algorithm can estimate up to $2(M-1)$ sources.

3 Cramer-Rao Bound

We derive the CRB of noncircular signals for double uniform linear arrays in this section. There are some differences between the CRB of noncircular signals DOA estimation and that of circular signals DOA estimation[17]. The parameters needed to estimate can be defined as

$$\boldsymbol{\zeta}=\begin{bmatrix}\theta_1,\cdots,\theta_K,\varphi_1,\cdots,\varphi_K,\boldsymbol{s}_{\mathrm{R}}^{\mathrm{T}}(t_1),\cdots,\\ \boldsymbol{s}_{\mathrm{R}}^{\mathrm{T}}(t_L),\boldsymbol{s}_{\mathrm{I}}^{\mathrm{T}}(t_1),\cdots,\boldsymbol{s}_{\mathrm{I}}^{\mathrm{T}}(t_L),\sigma^2\end{bmatrix}^{\mathrm{T}} \tag{52}$$

where $\boldsymbol{s}_{\mathrm{R}}(t_l)$ and $\boldsymbol{s}_{\mathrm{I}}(t_l)$ denote the real and imaginary parts of $\boldsymbol{s}(t_l)$, respectively.

According to Eq. (1), the sampled array output with L snapshots can be rewritten as

$$\boldsymbol{z}=[\boldsymbol{z}^{\mathrm{T}}(t_1),\cdots,\boldsymbol{z}^{\mathrm{T}}(t_L),\boldsymbol{z}^{\mathrm{H}}(t_1),\cdots,\boldsymbol{z}^{\mathrm{H}}(t_L)]^{\mathrm{T}} \tag{53}$$

where $\boldsymbol{z}(t_l)=[\boldsymbol{x}_1^{\mathrm{T}}(t_l),\boldsymbol{x}_2^{\mathrm{T}}(t_l)]^{\mathrm{T}}$, $\boldsymbol{x}_1(t_l)$ and $\boldsymbol{x}_2(t_l)$ are the samples of $\boldsymbol{x}_1(t_l)$ and $\boldsymbol{x}_2(t_l)$ at t_1, respectively.

The mean $\boldsymbol{\mu}$ and covariance $\boldsymbol{\Gamma}$ of $\boldsymbol{z}$ are

$$\boldsymbol{\mu}=\begin{bmatrix}\bar{\boldsymbol{A}}\boldsymbol{s}(t_1)\\ \vdots\\ \bar{\boldsymbol{A}}\boldsymbol{s}(t_L)\\ \bar{\boldsymbol{A}}^*\boldsymbol{s}^*(t_1)\\ \vdots\\ \bar{\boldsymbol{A}}^*\boldsymbol{s}^*(t_L)\end{bmatrix} \tag{54}$$

$$\boldsymbol{\Gamma}=\begin{bmatrix}\sigma^2\boldsymbol{I} & \cdots & \boldsymbol{0}\\ \vdots & \ddots & \vdots\\ \boldsymbol{0} & \cdots & \sigma^2\boldsymbol{I}\end{bmatrix} \tag{55}$$

where $\bar{\boldsymbol{A}}=[\boldsymbol{A}^{\mathrm{T}},\boldsymbol{\Phi}_{\mathrm{Y}}^{\mathrm{T}}\boldsymbol{A}^{\mathrm{T}}]^{\mathrm{T}}$.

From Ref. [30], the (i,j) element of the CRB matrix $\boldsymbol{P}$ can be expressed as

$$[\boldsymbol{P}^{-1}]_{ij}=\mathrm{tr}[\boldsymbol{\Gamma}^{-1}\boldsymbol{\Gamma}_i'\boldsymbol{\Gamma}^{-1}\boldsymbol{\Gamma}_j']+2\mathrm{Re}[\boldsymbol{\mu}_i'^{*}\boldsymbol{\Gamma}^{-1}\boldsymbol{\mu}_j'] \tag{56}$$

where $\boldsymbol{\mu}_i'$ and $\boldsymbol{\Gamma}_i'$ denote the first-order derivative of $\boldsymbol{\mu}$ and $\boldsymbol{\Gamma}$ with respect to the ith element of $\boldsymbol{\zeta}$, respectively.

For the covariance matrix $\boldsymbol{\Gamma}$ is just related to σ^2, the first term of Eq. (56) can be ignored. The (i,j) element of CRB matrix $\boldsymbol{P}$ can be simplified as

$$[\boldsymbol{P}^{-1}]_{ij}=2\mathrm{Re}[\boldsymbol{\mu}_i'^{*}\boldsymbol{\Gamma}^{-1}\boldsymbol{\mu}_j'] \tag{57}$$

According to Eqs. (52,54), we have

$$\frac{\partial \boldsymbol{\mu}}{\partial \theta_k}=\begin{bmatrix}\frac{\partial \bar{\boldsymbol{A}}}{\partial \theta_k}\boldsymbol{s}(t_1)\\ \vdots \\ \frac{\partial \bar{\boldsymbol{A}}}{\partial \theta_k}\boldsymbol{s}(t_L)\\ \frac{\partial \bar{\boldsymbol{A}}^*}{\partial \theta_k}\boldsymbol{s}^*(t_1)\\ \vdots \\ \frac{\partial \bar{\boldsymbol{A}}^*}{\partial \theta_k}\boldsymbol{s}^*(t_L)\end{bmatrix}=\begin{bmatrix}\boldsymbol{d}_{\theta_k}s_k(t_1)\\ \vdots \\ \boldsymbol{d}_{\theta_k}s_k(t_L)\\ \boldsymbol{d}^*_{\theta_k}s^*_k(t_1)\\ \vdots \\ \boldsymbol{d}^*_{\theta_k}s^*_k(t_L)\end{bmatrix} \tag{58}$$

$$\frac{\partial \boldsymbol{\mu}}{\partial \varphi_k}=\begin{bmatrix}\frac{\partial \bar{\boldsymbol{A}}}{\partial \varphi_k}\boldsymbol{s}(t_1)\\ \vdots \\ \frac{\partial \bar{\boldsymbol{A}}}{\partial \varphi_k}\boldsymbol{s}(t_L)\\ \frac{\partial \bar{A}^*}{\partial \varphi_k}\boldsymbol{s}^*(t_1)\\ \vdots \\ \frac{\partial \bar{\boldsymbol{A}}^*}{\partial \varphi_k}\boldsymbol{s}^*(t_L)\end{bmatrix}=\begin{bmatrix}\boldsymbol{d}_{\varphi_k}s_k(t_1)\\ \vdots \\ \boldsymbol{d}_{\varphi_k}s_k(t_L)\\ \boldsymbol{d}^*_{\varphi_k}s^*_k(t_1)\\ \vdots \\ \boldsymbol{d}^*_{\varphi_k}s^*_k(t_L)\end{bmatrix} \tag{59}$$

where $s_k(t_l)$ is the kth element of $\boldsymbol{s}(t_l)$, and

$$\boldsymbol{d}_{\theta_k}=\frac{\partial \bar{\boldsymbol{a}}_k}{\partial \theta_k} \tag{60}$$

$$\boldsymbol{d}_{\varphi_k}=\frac{\partial \bar{\boldsymbol{a}}_k}{\partial \varphi_k} \tag{61}$$

where $\bar{\boldsymbol{a}}_k$ is the kth column vector of $\bar{\boldsymbol{A}}$.

Define

$$\boldsymbol{s}=\begin{bmatrix}\boldsymbol{s}(t_1)\\ \vdots \\ \boldsymbol{s}(t_L)\end{bmatrix} \tag{62}$$

$$\boldsymbol{G}=\begin{bmatrix}\bar{\boldsymbol{A}} & \cdots & \boldsymbol{0}\\ \vdots & \ddots & \vdots \\ \boldsymbol{0} & \cdots & \bar{\boldsymbol{A}}\end{bmatrix} \tag{63}$$

$$\boldsymbol{\Delta}=[\boldsymbol{\Delta}_\theta,\boldsymbol{\Delta}_\varphi] \tag{64}$$

where

$$\boldsymbol{\Delta}_\theta=\begin{bmatrix}\boldsymbol{d}_{\theta_1}s_1(t_1) & \cdots & \boldsymbol{d}_{\theta_K}s_K(t_1)\\ \vdots & \ddots & \vdots \\ \boldsymbol{d}_{\theta_1}s_1(t_L) & \cdots & \boldsymbol{d}_{\theta_K}s_K(t_L)\end{bmatrix}$$

$$\boldsymbol{\Delta}_\varphi=\begin{bmatrix}\boldsymbol{d}_{\varphi_1}s_1(t_1) & \cdots & \boldsymbol{d}_{\varphi_K}s_K(t_1)\\ \vdots & \ddots & \vdots \\ \boldsymbol{d}_{\varphi_1}s_1(t_L) & \cdots & \boldsymbol{d}_{\varphi_K}s_K(t_L)\end{bmatrix}$$

Then we have

$$\boldsymbol{\mu}=\begin{bmatrix}\boldsymbol{G}\boldsymbol{s}\\ \boldsymbol{G}^*\ \boldsymbol{s}^*\end{bmatrix} \tag{65}$$

$$\frac{\partial \boldsymbol{\mu}}{\partial \boldsymbol{s}_{\mathrm{R}}^{\mathrm{T}}}=\begin{bmatrix}\boldsymbol{G}\\ \boldsymbol{G}^*\end{bmatrix} \tag{66}$$

$$\frac{\partial \boldsymbol{\mu}}{\partial \boldsymbol{s}_{\mathrm{I}}^{\mathrm{T}}}=\begin{bmatrix}\mathrm{j}\boldsymbol{G}\\ -\mathrm{j}\boldsymbol{G}^*\end{bmatrix} \tag{67}$$

Combining Eq. (52) and Eqs. (62)—(67), the first-order derivative of $\boldsymbol{\mu}$ with respect to $\boldsymbol{\zeta}$ is

$$\frac{\partial \boldsymbol{\mu}}{\partial \boldsymbol{\zeta}^{\mathrm{T}}}=\begin{bmatrix}\boldsymbol{\Delta} & \boldsymbol{G} & \mathrm{j}\boldsymbol{G} & \boldsymbol{0}\\ \boldsymbol{\Delta}^* & \boldsymbol{G}^* & -\mathrm{j}\boldsymbol{G}^* & \boldsymbol{0}\end{bmatrix} \tag{68}$$

Combine Eq. (55) with Eq. (68), and Eq. (57)can be rewritten as

$$2\mathrm{Re}\left[\frac{\partial \boldsymbol{\mu}^*}{\partial \boldsymbol{\zeta}}\boldsymbol{\Gamma}^{-1}\ \frac{\partial \boldsymbol{\mu}}{\partial \boldsymbol{\zeta}^{\mathrm{T}}}\right]=\begin{bmatrix}\boldsymbol{J} & \boldsymbol{0}\\ \boldsymbol{0} & \boldsymbol{0}\end{bmatrix} \tag{69}$$

where

$$\boldsymbol{J}=\frac{2}{\sigma^2}\mathrm{Re}\left\{\begin{bmatrix}\boldsymbol{\Delta}^{\mathrm{H}} & \boldsymbol{\Delta}^{\mathrm{T}}\\ \boldsymbol{G}^{\mathrm{H}} & \boldsymbol{G}^{\mathrm{T}}\\ -\mathrm{j}\boldsymbol{G}^{\mathrm{H}} & \mathrm{j}\boldsymbol{G}^{\mathrm{T}}\end{bmatrix}\begin{bmatrix}\boldsymbol{\Delta} & \boldsymbol{G} & \mathrm{j}\boldsymbol{G}\\ \boldsymbol{\Delta}^* & \boldsymbol{G}^* & -\mathrm{j}\boldsymbol{G}^*\end{bmatrix}\right\}$$

Let

$$\boldsymbol{B}\triangleq(\boldsymbol{G}^{\mathrm{H}}\boldsymbol{G})^{-1}\boldsymbol{G}^{\mathrm{H}}\boldsymbol{\Delta} \tag{70}$$

$$\boldsymbol{F}\triangleq\begin{bmatrix}\boldsymbol{I} & \boldsymbol{0} & \boldsymbol{0}\\ -\boldsymbol{B}_{\mathrm{R}} & \boldsymbol{I} & \boldsymbol{0}\\ -\boldsymbol{B}_{\mathrm{I}} & \boldsymbol{0} & \boldsymbol{I}\end{bmatrix} \tag{71}$$

where $\boldsymbol{B}_{\mathrm{R}}$ and $\boldsymbol{B}_{\mathrm{I}}$ are the real and imaginary parts of $\boldsymbol{B}$, respectively.

According to Eqs. (69)—(71), we have

$$[\boldsymbol{\Delta}\quad\boldsymbol{G}\quad\mathrm{j}\boldsymbol{G}]\boldsymbol{F}=[\boldsymbol{\Pi}_{\mathrm{G}}^{\perp}\boldsymbol{\Delta}\quad\boldsymbol{G}\quad\mathrm{j}\boldsymbol{G}] \tag{72}$$

$$[\boldsymbol{\Delta}^*\quad\boldsymbol{G}^*\quad-\mathrm{j}\boldsymbol{G}^*]\boldsymbol{F}=[\boldsymbol{\Pi}_{\mathrm{G}^*}^{\perp}\boldsymbol{\Delta}^*\boldsymbol{G}^*\quad-\mathrm{j}\boldsymbol{G}^*] \tag{73}$$

where $\boldsymbol{\Pi}_{\mathrm{G}}^{\perp}=\boldsymbol{I}-\boldsymbol{G}(\boldsymbol{G}^{\mathrm{H}}\boldsymbol{G})^{-1}\boldsymbol{G}^{\mathrm{H}}$, $\boldsymbol{G}^{\mathrm{H}}\boldsymbol{\Pi}_{\mathrm{G}}^{\perp}=\boldsymbol{0}$.

Thus, it can be demonstrated that

$$\boldsymbol{F}^{\mathrm{T}}\boldsymbol{J}\boldsymbol{F}=\frac{2}{\sigma^2}\mathrm{Re}\left\{\boldsymbol{F}^{\mathrm{H}}\begin{bmatrix}\boldsymbol{\Delta}^{\mathrm{H}} & \boldsymbol{\Delta}^{\mathrm{T}}\\ \boldsymbol{G}^{\mathrm{H}} & \boldsymbol{G}^{\mathrm{T}}\\ -\mathrm{j}\boldsymbol{G}^{\mathrm{H}} & \mathrm{j}\boldsymbol{G}^{\mathrm{T}}\end{bmatrix}\begin{bmatrix}\boldsymbol{\Delta} & \boldsymbol{G} & \mathrm{j}\boldsymbol{G}\\ \boldsymbol{\Delta}^* & \boldsymbol{G}^* & -\mathrm{j}\boldsymbol{G}^*\end{bmatrix}\boldsymbol{F}\right\}=$$

$$\frac{2}{\sigma^2}\mathrm{Re}\left\{\begin{bmatrix}\boldsymbol{\Delta}^{\mathrm{H}}\boldsymbol{\Pi}_{\mathrm{G}}^{\perp} & \boldsymbol{\Delta}^{\mathrm{T}}\boldsymbol{\Pi}_{G}^{\perp}\\ \boldsymbol{G}^{\mathrm{H}} & \boldsymbol{G}^{\mathrm{T}}\\ -\mathrm{j}\boldsymbol{G}^{\mathrm{H}} & \mathrm{j}\boldsymbol{G}^{\mathrm{T}}\end{bmatrix}\begin{bmatrix}\boldsymbol{\Pi}_{\mathrm{G}}^{\perp}\boldsymbol{\Delta} & \boldsymbol{G} & \mathrm{j}\boldsymbol{G}\\ \boldsymbol{\Pi}_{\boldsymbol{G}^*}^{\perp}\boldsymbol{\Delta}^* & \boldsymbol{G}^* & -\mathrm{j}\boldsymbol{G}^*\end{bmatrix}\right\}=$$

$$\frac{4}{\sigma^2}\mathrm{Re}\left\{\begin{bmatrix}\boldsymbol{\Delta}^{\mathrm{H}}\boldsymbol{\Pi}_{\mathrm{G}}^{\perp}\boldsymbol{\Delta} & \boldsymbol{0} & \boldsymbol{0}\\ \boldsymbol{0} & \boldsymbol{G}^{\mathrm{H}}\boldsymbol{G} & \mathrm{j}\boldsymbol{G}^{\mathrm{H}}\boldsymbol{G}\\ \boldsymbol{0} & -\mathrm{j}\boldsymbol{G}^{\mathrm{H}}\boldsymbol{G} & \boldsymbol{G}^{\mathrm{H}}\boldsymbol{G}\end{bmatrix}\right\} \tag{74}$$

Only the elements related to the angles are considered. According to Eq. (74), $\boldsymbol{J}^{-1}$ can be expressed as

$$\boldsymbol{J}^{-1}=\boldsymbol{F}(\boldsymbol{F}^{\mathrm{T}}\boldsymbol{J}\boldsymbol{F})^{-1}\boldsymbol{F}^{\mathrm{T}}=$$

$$\frac{\sigma^2}{4}\begin{bmatrix}\boldsymbol{I} & \boldsymbol{0}\ \boldsymbol{0}\\ -\boldsymbol{B}_{\mathrm{R}} & \boldsymbol{I}\ \boldsymbol{0}\\ -\boldsymbol{B}_{\mathrm{I}} & \boldsymbol{0}\ \boldsymbol{I}\end{bmatrix}\begin{bmatrix}\mathrm{Re}(\boldsymbol{\Delta}^{\mathrm{H}}\boldsymbol{\Pi}_{\boldsymbol{G}}^{\perp}\boldsymbol{\Delta}) & \boldsymbol{0}\ \boldsymbol{0}\\ \boldsymbol{0} & \boldsymbol{\kappa}\ \boldsymbol{\kappa}\\ \boldsymbol{0} & \boldsymbol{\kappa}\ \boldsymbol{\kappa}\end{bmatrix}\begin{bmatrix}\boldsymbol{I} & \boldsymbol{0}\ \boldsymbol{0}\\ -\boldsymbol{B}_{\mathrm{R}} & \boldsymbol{I}\ \boldsymbol{0}\\ -\boldsymbol{B}_{\mathrm{I}} & \boldsymbol{0}\ \boldsymbol{I}\end{bmatrix}=$$

$$\begin{bmatrix} \frac{\sigma^2}{4}\left[\mathrm{Re}(\boldsymbol{\Delta}^{\mathrm{H}}\boldsymbol{\Pi}_{\mathrm{G}}^{\perp}\boldsymbol{\Delta})\right]^{-1} & \boldsymbol{\kappa}\ \boldsymbol{\kappa} \\ \boldsymbol{\kappa} & \boldsymbol{\kappa}\ \boldsymbol{\kappa} \\ \boldsymbol{\kappa} & \boldsymbol{\kappa}\ \boldsymbol{\kappa} \end{bmatrix} \tag{75}$$

where $\boldsymbol{\kappa}$ denotes the parts unrelated to the elevation angles and azimuth angles.

Thus, the CRB matrix can be obtained as

$$\mathrm{CRB}=\frac{\sigma^2}{4}\left[\mathrm{Re}(\boldsymbol{\Delta}^{\mathrm{H}}\boldsymbol{\Pi}_{\mathrm{G}}^{\perp}\boldsymbol{\Delta})\right]^{-1} \tag{76}$$

After further simplification, the CRB matrix can be rewritten as

$$\mathrm{CRB}=\frac{\sigma^2}{4L}\{\mathrm{Re}[\boldsymbol{D}^{\mathrm{H}}\boldsymbol{\Pi}_{\bar{\boldsymbol{A}}}^{\perp}\boldsymbol{D}\odot\boldsymbol{P}_s^{\mathrm{T}}]\}^{-1} \tag{77}$$

where $\boldsymbol{D}=\left[\frac{\partial\bar{\boldsymbol{a}}_1}{\partial\theta_1},\cdots,\frac{\partial\bar{\boldsymbol{a}}_K}{\partial\theta_K},\frac{\partial\bar{\boldsymbol{a}}_1}{\partial\varphi_1},\cdots,\frac{\partial\bar{\boldsymbol{a}}_K}{\partial\varphi_K}\right]$, σ^2 is the power of noise, $\odot$ denotes the Hadamard product, $\boldsymbol{\Pi}_{\bar{\boldsymbol{A}}}^{\perp}=\boldsymbol{I}_{4M}-\bar{\boldsymbol{A}}(\bar{\boldsymbol{A}}^{\mathrm{H}}\bar{\boldsymbol{A}})^{-1}\bar{\boldsymbol{A}}^{\mathrm{H}}$, and $\boldsymbol{P}_s=\frac{1}{L}\cdot\sum_{l=1}^{L}\boldsymbol{s}(t_l)\boldsymbol{s}(t_l)^{\mathrm{H}}$.

4 Simulation Results

The Monte Carlo simulations are adopted to evaluate the angle estimation performance of the proposed algorithm. The rootmean square error (RMSE) is defined as[31]

$$\mathrm{RMSE}=\frac{1}{K}\sum_{k=1}^{K}\sqrt{\frac{1}{N}\sum_{n=1}^{N}(\hat{\alpha}_{k,n}-\alpha_k)^2} \tag{78}$$

where $\hat{\alpha}_{k,n}$ is the estimate of θ_k/φ_k of the nth Monte Carlo trial. $N=300$ is the number of simulation loops. Assume that all sources have the same symbol duration and the same input signal-to-noise ratio (SNR). The signals are all BPSK modulated. The distance between adjacent sensors is equivalent to half of the wavelength, $d=\lambda/2$. Simulation results are shown in Figs. 3—8.

In the following simulation results except Figs. 4, 7, 8, we assume that there are $K=3$ sources located at angles of $(\theta_1,\theta_2,\theta_3)=(15°,35°,55°)$ and $(\varphi_1,\varphi_2,\varphi_3)=(10°,30°,50°)$. The noncircular phases are $(\psi_1,\psi_2,\psi_3)=(20°,40°,60°)$, respectively.

Fig. 3 presents angle estimation result of elevation angles and azimuth angles of the proposed algorithm. $M=8$ and $L=300$ are used in the simulations, while SNR = 10 dB. From Fig. 3, the elevation angles and azimuth angles can be clearly observed.

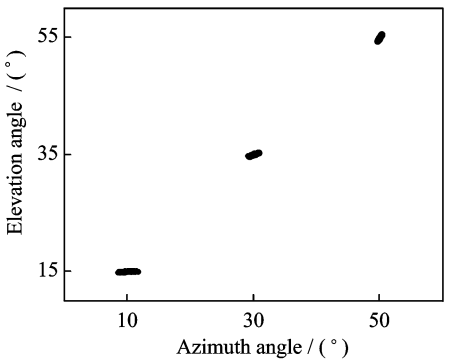

Fig. 3 Angle estimation result over Monte Carlo simulations

Fig. 4 shows the angle estimation performance comparison among the proposed algorithm, 2D ESPRIT algorithm[10], 2D NC-ESPRIT algorithm[14], 2D NC-PM algorithm[22], and CRB of noncircular signals for double parallel uniform linear arrays. $M=6$, $K=2$ and $L=300$ are used in the simulations. From Fig. 4, it is indicated that the angle estimation performance of the proposed algorithm is close to that of 2D NC-ESPRIT algorithm and better than that of the other 2D angle estimation algorithms, since the effective array aperture is doubled by exploiting the noncircularity of signals.

Fig. 5 shows angle estimation performance of the proposed algorithm with $L=300$ and different values of M. From Fig. 5, it can be seen that the increasing of M will lead to the improvement of angle estimation performance of the proposed algorithm.

Fig. 6 depicts angle estimation performance of the proposed algorithm with $M=8$ and different values of L. From Fig. 6, the angle estimation performance of the proposed algorithm is enhanced with the number of snapshots increasing.

Fig. 7 presents angle estimation performance of the proposed algorithm with $M=8$, $L=300$ and different values of K. From Fig. 7, it can be found that the angle estimation performance of the proposed algorithm degrades with the number of source increasing.

Fig. 8 displays the simulation result of the proposed algorithm with two closely spaced sources. In Fig. 8, we assume that the two closely spaced sources are located at angles of $(\theta_1, \theta_2) = (30°, 32°)$ and $(\varphi_1, \varphi_2) = (10°, 12°)$. The corresponding noncircular phases are $(\psi_1, \psi_2) = (20°, 40°)$, respectively. $M = 10$, $L = 500$ and SNR = 20 dB are used in the simulation. Fig. 8 implies that the proposed algorithm works well when two sources are closely spaced.

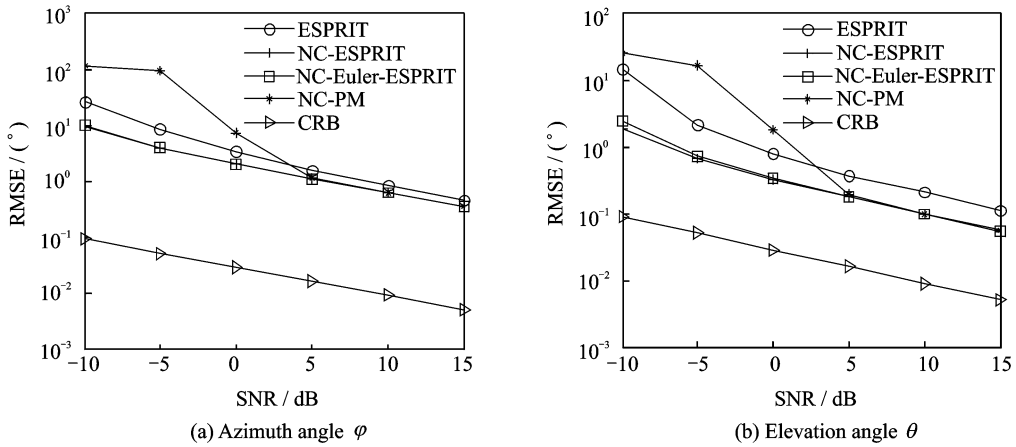

Fig. 4 Simulation results of angle estimation performance comparison

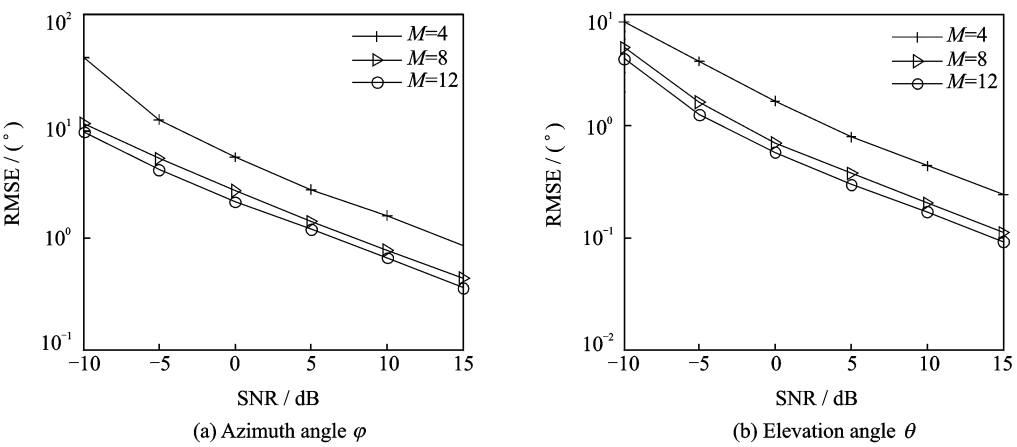

Fig. 5 Angle estimation performances with different values of M

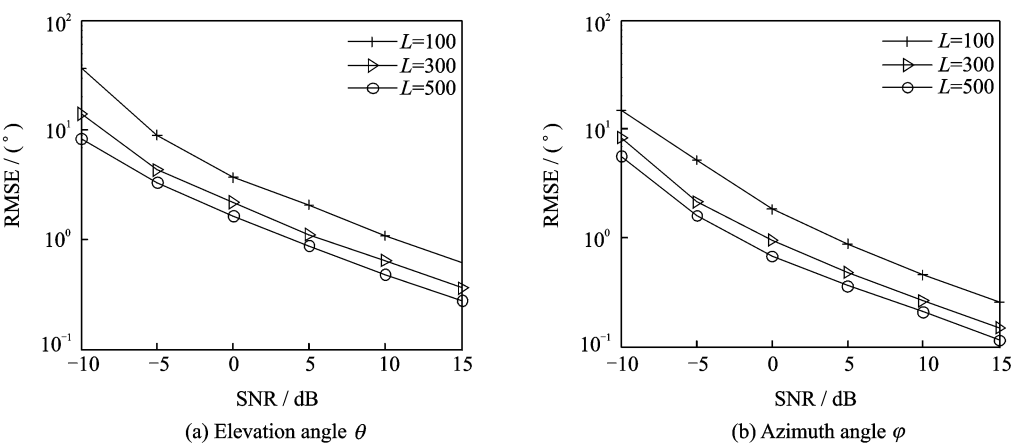

Fig. 6 Angle estimation performances with different values of L

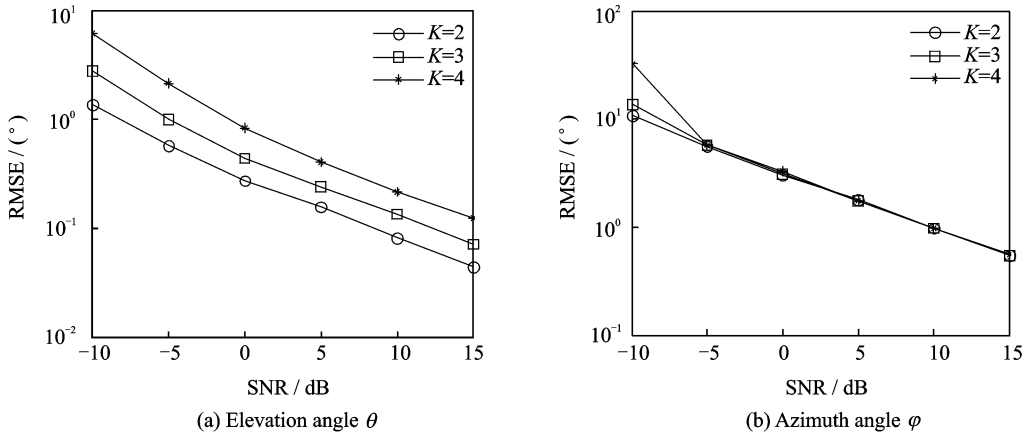

Fig. 7 Angle estimation performances with different values of K

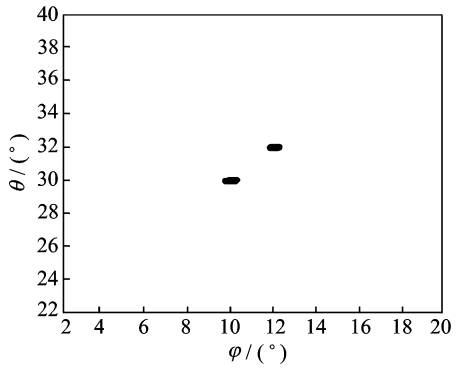

Fig. 8 Angle estimation result of two closely spaced sources

5 Conclusions

In this paper, we have proposed a real-valued 2D NC-Euler-RI algorithm of noncircular signals for double parallel uniform linear arrays. The proposed algorithm has the following advantages:

(1) It has much lower computational complexity than that of 2D NC-ESPRIT algorithm[14] for double parallel uniform linear arrays.

(2) It has better angle estimation performance than that of 2D ESPRIT algorithm[10] and 2D NC-PM algorithm[22] for double parallel uniform linear arrays, and very close to that of 2D NC-ESPRIT algorithm[14] for double parallel uniform linear arrays.

(3) It can estimate elevation angles and azimuth angles with automatically pairing.

(4) The maximum number of source estimated by the proposed algorithm is two times that of 2D ESPRIT algorithm, for the effective array aperture is doubled via utilizing the noncircularity of signal.

We also analyze the computational complexity of the proposed algorithm. The CRB of noncircular signals for double parallel uniform linear arrays are also derived. It is well known that CRB expresses a lower bound on the variance of an unbiased estimator, which can be used to compare the angle performance of different algorithms. From Fig. 4, it can be seen that the RMSE of the proposed 2D NC-Euler-RI algorithm is much closer to CRB compared with that of 2D ESPRIT algorithm and 2D NC-PM algorithm. It is also clearly indicated that the angle estimation performance of our algorithm is better than that of 2D ESPRIT algorithm and 2D NC-PM algorithm. Finally, the angle estimation performance and computational complexity of the proposed algorithm are evaluated by numerical simulations. Simulation results illustrate the effectiveness of the proposed algorithm in a variety of scenarios, even when the sources are closely spaced.

Acknowledgements

This work is supported by the National Science Foundation of China (No. 61371169) and the Aeronautical Science Foundation of China (No. 20120152001).

References:

[1] KRIM H, VIBERG M. Two decades of array signal processing research: The parametric approach [J]. IEEE Signal Processing Magazine, 1996, 13(4): 67-94.

[2] CHEN W Y, ZHANG X F, ZHANG L C. DOA tracking algorithm for acoustic vector-sensor array via Kalman filter and OPASTd[J]. Journal of Nanjing University of Aeronautics & Astronautics, 2015,47(3):377-383. (in Chinese)

[3] LI J F, ZHANG X F, CHEN W Y, et al. Reduced-dimensional ESPRIT for direction finding in monostatic MIMO radar with double parallel uniform linear arrays [J]. Wireless Personal Communications, 2014,77(1):1-19.

[4] FU W B, ZHAO Y B, SU T, et al. DOA matrix method based on MIMO radar with L-shape arrays [J]. System Engineering and Electronics, 2011,33(11):2398-2403.

[5] ZHANG X F, ZHANG L C, CHEN W Y, et al. Computationally efficient DOA estimation for MIMO array using propagator method and reduced-dimension transformation[J]. Journal of Data Acquisition and Processing, 2014,29(3):372-377.

[6] KHABBAZIBASMENJ A, HASSANIEN A, VOROBYOV S A, et al. Efficient transmit beamspace design for search-free based DOA estimation in MIMO radar[J]. IEEE Transactions on Signal Processing, 2014,62(6):1490-1500.

[7] BRESLER Y, MACOVSKI A. Exact maximum likelihood parameter estimation of super-imposed exponential signals in noise[J]. IEEE Transactions on Acoustics, Speech, and Signal Processing, 1986,34(5):1081-1089.

[8] ZISKIND I, WAX M. Maximum likelihood localization of multiple sources by alternating projection[J]. IEEE Transactions on Acoustics, Speech, and Signal Processing, 1988,36(10):1553-1560.

[9] SCHMIDT R O. Multiple emitter location and signal parameter estimation[J]. IEEE Transactions on Antennas and Propagation, 1986,AP-34(3):276-280.

[10] KAILATH T, ROY R. ESPRIT-estimation of signal parameters via rotational invariance techniques[J]. Optical Engineering, 1989,29(4):984-995.

[11] BARBARESCO F, CHEVALIER P. Noncircularity exploitation in signal processing overview and application to radar[C]//IET Waveform Diversity and Digital Radar Conference. London, UK: IET Seminar Digest, 2008:1-6.

[12] DELMAS J P, ABEIDA H. Cramer-Rao bounds of DOA estimates for BPSK and QPSK modulated signals[J]. IEEE Transactions on Signal Processing, 2006,54(1):117-126.

[13] CHARGE P, WANG Y, SAILLARD J. A root-MUSIC algorithm for non circular sources[C]//IEEE International Conference on Acoustics, Speech and Signal Processing. Salt Lake City, UT, USA: IEEE, 2001:2985-2988.

[14] ZOUBIR A, CHARGE P, WANG Y. Non circular sources localization with ESPRIT[C]//The 6th European Conference on Wireless Technology. Munich, Germang: Horizon House Publication LTD, 2003:736-744.

[15] WANG W, WANG X P, LI X. Propagator method for angle estimation of non-circular sources in Bistatic MIMO radar[C]//IEEE Radar Conference. Ottawa, ON, Canada: IEEE, 2013:1-5.

[16] SUN X Y, ZHOU J J. PM method for noncircular signals[J]. Journal of Data Acquisition and Processing, 2013,28(3):313-318.

[17] ZHANG X F, CAO R A, ZHOU M. Noncircular-PARAFAC for 2D-DOA estimation of noncircular signals in arbitrarily spaced acoustic vector-sensor array subjected to unknown locations[J]. EURASIP Journal on Advances in Signal Processing, 2012,2013(1):1-10.

[18] HUARNG K C, YEH C C. A unitary transformation method for angle-of-arrival estimation[J]. IEEE Transactions on Signal Processing, 1991,39(4):975-977.

[19] HAARDT M, NOSSEK J. Unitary ESPRIT: How to obtain increased estimation accuracy with a reduced computational burden[J]. IEEE Transactions on Signal Processing, 1995,43(5):1232-1242.

[20] ZHENG C D, FENG D Z, ZHOU W, et al. A real-value algorithm of ESPRIT via exploitation of non-circular sources property[J]. Journal of Electronics & Information Technology, 2008,30(1):130-133.

[21] ZHANG X F, ZHANG L C, SUN H P, et al. Two-dimensional DOA estimation algorithm for two parallel linear array via Euler transformation and propagator method [J]. Journal of Nanjing University of Aeronautics & Astronautics, 2015,47(3):324-331. (in Chinese)

[22] CHEN X Q, WANG C H, ZHANG X F. DOA and noncircular phase estimation of noncircular signal via an improved noncircular rotational invariance propagator method[J]. Mathematical Problems in Engineering, 2015(8):DOI:10.1155/2015/235173.

[23] YIN Q Y, NEWCOMB R W, ZOU L H. Estimating 2-D angles of arrival via two parallel linear arrays [C]//International Conference on Acoustics, Speech, and Signal Processing. Glasgow, UK:

IEEE, 1989:2803-2806.

[24] WEN F, WAN Q. Maximum likelihood and signal-selective TDOA estimation for noncircular signals [J]. Journal of Communications and Networks, 2013,15(3):245-251.

[25] XIA T Q, ZHENG Y, WAN Q, et al. 2-D angle-of-arrival estimation with two parallel uniform linear arrays[C]//IEEE Radar Conference. Shanghai, China: IEEE, 2006:244-247.

[26] ZHANG X F, XU L Y, XU L, et al. Direction of departure (DOD) and direction of arrival (DOA) estimation in MIMO radar with reduced-dimension MUSIC[J]. IEEE Communications Letters, 2010,14(12):1161-1163.

[27] CHEN P, WICKS M C, ADVE R S. Development of a statistical procedure for detecting the number of signals in a radar measurement[J]. IEEE Proceeding of Radar, Sonar and Navigation, 2001,148(4):219-226.

[28] XIN J M, ZHENG N N, Sano A. Simple and efficient nonparametric method for estimating the number of signals without Eigen-decomposition[J]. IEEE Transactions on Signal Processing, 2007, 55(4): 1405-1420.

[29] CHUNG W H, CHEN C E. Detecting number of coherent signals in array processing by Ljung-box statistic[J]. IEEE Transactions on Aerospace and Electronic Systems, 2012,48(2):1739-1747.

[30] STOICA P, NEHORAI A. Performance study of conditional and unconditional direction-of-arrival estimation [J]. IEEE Transactions on Acoustics, Speech, and Signal Processing, 1990,38(10):1783-1795.

[31] LI J F, ZHANG X F. Two-dimensional angle estimation for monostatic MIMO arbitrary array with velocity receiver sensors and unknown locations[J]. Digital Signal Processing, 2014,24:34-41.

Dr. **Chen Xueqiang** received B. S. degree from Qi Lu University of Technology, Jinan, China, in 2008, and the Ph. D. degree in College of Electronic and Information Engineering, Nanjing University of Aeronautics & Astronautics, Nanjing, China. He is currently a lecturer in College of Communication Engineeringof Army Engineering University. His research interest focuses on array signal processing and communication signal processing.

Prof. **Wang Chenghua** received B. S. degree and M. S. degree from Southeast University, Nanjing, China, in 1984 and 1987, respectively. He is currently a professor in college of electronic and information engineering at Nanjing University of Aeronautics & Astronautics, Nanjing, China. His research interest focuses on circuits and systems, communication and information systems.

Prof. **Zhang Xiaofei** received M. S. degree from Wuhan University in 2001, and the Ph. D. degree in communication and information systems from Nanjing University of Aeronautics and Astronautics in 2005. Now, he is a professor in electronic engineering department, Nanjing University of Aeronautics & Astronautics, Nanjing, China. His research interest focuses on array signal processing and communication signal processing.

(Production Editor: Zhang Huangqun)